Available online at www.CivileJournal.org

Civil Engineering Journal

(E-ISSN: 2476-3055; ISSN: 2676-6957)

Vol. 10, No. 10, October, 2024

Refining Low Strain Pile Integrity Testing for Minor Flaw Detection with Complex Wavelet Transform

Elizaveta Loseva [1], Ilya Lozovsky [2*], Ruslan Zhostkov [3]

[1] *Empress Catherine II Saint Petersburg Mining University, 199106 2, 21st Line, St. Petersburg, Russia.*

[2] *Geoelectromagnetic Research Center–Branch of Schmidt Institute of Physics of the Earth of the Russian Academy of Sciences, Troitsk, 108840 Moscow, Russia.*

[3] *Schmidt Institute of Physics of the Earth of the Russian Academy of Sciences, 123995 Moscow, Russia.*

Received 28 May 2024; Revised 23 September 2024; Accepted 29 September 2024; Published 01 October 2024

Abstract

The structural integrity of pile foundations is critical for the safety and longevity of buildings and infrastructure. Low strain impact testing is a widely used non-destructive method for assessing pile length and identifying significant defects; however, its sensitivity to minor flaws remains limited. This study aims to enhance the detection capabilities of low strain testing for minor defects by proposing an improved methodology. We conducted field tests on ten piles with small, artificially introduced flaws and complemented these tests with three-dimensional numerical simulations. Initial time-domain analyses of both field and simulated data, using low-frequency wave excitation, did not reveal distinct signal features indicative of defects. To address this limitation, we employed a set of hammers with varying weights and head materials for wave excitation, simulated with different input force pulse durations. We further applied Complex Continuous Wavelet Transform (CCWT) for time-frequency analysis of the acquired signals, which effectively identified minor defects through characteristic changes in wavelet coefficient phase angles at expected timestamps. The consistency of CCWT phase spectrum features across signals from different hammers, considering the varying sensitivities of wave excitations, facilitates the differentiation of genuine flaw-induced phase shifts from noise. The study's findings were integrated into an improved low strain pile integrity testing workflow, enhancing the method's accuracy in detecting minor flaws.

Keywords: Piles; Cast-in-Place Piles; Non-destructive Testing; NDT; Pile Integrity Testing; Low Strain Integrity Testing; Numerical Simulations; Wavelet Analysis; Continuous Wavelet Transform; Morlet Wavelet.

1. Introduction

Modern urban planning increasingly prioritizes vertical construction to optimize land use, thereby conserving valuable surface space. The safety and functionality of high-rise buildings and critical infrastructure depend on precise foundation design. In this context, pile foundations have become a preferred choice due to their proven capacity to support substantial loads and maintain structural stability, making them essential across various construction scenarios [1]. Pile foundations are especially beneficial in challenging engineering and geological conditions, such as construction on permafrost [2-4] and in the oil [5-7] and energy industries [8].

Ensuring the quality of these pile foundations is as crucial as their design. Consequently, there is growing demand for non-destructive testing (NDT) methods, such as low strain integrity testing (sonic-echo, PIT, PET) [9, 10]. This test method relies on analyzing elastic wave propagation within a pile shaft, facilitating quality control of concealed work, timely detection of defects, and verification of pile length. Despite its widespread use, the method has several notable

* Corresponding author: i.n.lozovsky@yandex.ru

http://dx.doi.org/10.28991/CEJ-2024-010-10-05

limitations [11]. According to ASTM D5882, while this method is effective for detecting major defects, it may not identify all imperfections within a pile [12]. Minor flaws, however, can substantially impact the structural integrity of piles [13,14]. Therefore, it is essential to develop techniques that enhance the method's ability to detect minor defects. Addressing this issue requires the advancement of testing methods to improve their resolution and sensitivity.

Commercial software for evaluating pile length and integrity often employs Fourier Transform (FT) filtering to denoise data. While FT is effective at identifying and removing unwanted frequencies, it lacks time resolution, meaning it can determine which frequencies are present but not when they occur [15]. To address this limitation, Dennis Gabor introduced the *Gabor Transform*, which uses a Gaussian window function to provide time-frequency analysis by combining time and frequency information in a single representation [16]. The Short-Time Fourier Transform (STFT) was developed to achieve time-frequency analysis by applying a series of different window functions to segments of the signal. However, STFT comes with trade-offs: smaller windows improve time resolution but reduce frequency precision, while larger windows enhance frequency resolution but diminish time accuracy [17]. Jean Morlet enhanced time-frequency analysis by introducing wavelets, building on the concepts of the STFT. He created the Morlet wavelet, which, like the Gabor Transform, uses a Gaussian-shaped function but allows for varying scales to balance time and frequency resolution. Morlet proposed a family of wavelets derived from a "mother wavelet" that can be scaled to capture both low- and high-frequency characteristics of signals [18].

The wavelet transform, originally developed for seismic data analysis, remains a powerful tool in seismic exploration [19], as well as in gravity [20], and electromagnetic [21] geophysical data analysis. In civil engineering, wavelet transforms are employed for analyzing earthquake-induced vibrations, bridge vibrations [22], and non-destructive testing of structures [23, 24]. Addison & Watson [25] and Watson et al. [26] first applied the wavelet transform to low strain pile integrity testing, using it to denoise data derived from finite element simulations. Wang extended this technique to detect defects such as necking and concrete separation [27]. Ni et al. utilized wavelet transforms in field experiments to estimate the depth of long piles, measuring pile toe depth up to 50 meters [28]. Additionally, Ni et al. used the discrete wavelet transform to detect defects in small hollow piles [29]. Recent work by Ni et al. has advanced these methods by introducing complex wavelets, which enhance defect detection by providing a more detailed representation of the phase spectrum and capturing subtle changes in both frequency and phase across different scales [30, 31]. Zheng et al. investigated the sensitivity of wavelet phase spectrum analysis to defects at various depths [32]. Liu et al. further advanced this field by introducing an enhanced algorithm for defect localization, incorporating CCWT phase angle turning points along with tools such as K-means clustering and fast Fourier transform [33].

The literature shows that wavelet transforms are commonly used for estimating pile length and detecting defects. However, many studies rely solely on numerical simulations or field tests of piles with unknown characteristics and do not fully assess the reliability of these techniques for detecting minor defects. To address this, our study aims to evaluate the sensitivity of CCWT phase analysis for identifying minor defects in cast-in-place piles. We will enhance our approach by incorporating data from hammers with different weights and head materials. Our analysis will involve both numerical simulations and field tests on specially constructed piles with small artificial defects, aiming to improve the detection capabilities of low-strain testing for minor defects.

2. Material and Methods

2.1. Defects in Pile Foundations

Piles are broadly categorized into two types based on their installation methods: precast and cast-in-place. Precast piles can develop defects during the driving process, such as cracks and issues with section splicing [34, 35]. Cast-in-place piles, on the other hand, are vulnerable to defects arising from deviations in construction procedures (drilling, concreting, and reinforcing) and environmental factors before the concrete hardens. These defects may compromise the pile's load-bearing capacity and durability, highlighting the need for reliable non-destructive testing [36, 37]. The most common types of defects (Figure 1), along with their causes [38], are outlined below:

- Necking refers to a reduction in the pile cross-section, which can occur locally over a few centimeters in height or extend along several meters. Typically, necking results in a reduced pile diameter around the reinforcement cage, with the concrete inside the cage being less affected. This defect often arises from natural forces or errors in the concreting process.
- Washout refers to the erosion of the concrete mixture's integrity, usually due to challenging hydrogeological conditions. This defect is most common in sandy or gravelly soils with significant water flow. Washout is characterized by the absence of cement in the pile shaft, as water currents partially or entirely wash it away before the concrete hardens, leaving behind only coarse or fine aggregate.
- Soil inclusion occurs when large soil particles infiltrate the pile shaft after concreting, compromising its integrity. This defect typically results from the sliding of borehole walls into the shaft, often due to deviations in the pile concreting process.

Figure 1. Common defects in cast-in-place piles: necking, washout, and soil inclusion (from left to right)

2.2. Low Strain Integrity Testing

Non-destructive testing methods are extensively employed across various fields to evaluate the properties of materials, structures, or components without causing any physical damage [39-41]. Among these methods, low strain integrity testing is used for assessing the integrity of augered cast-in-place piles, drilled shafts, and precast piles. This technique involves analyzing the velocity response of the pile induced by a handheld hammer blow (Figure 2). Governed by ASTM D5882 standard [12] and other international codes, it is one of the most commonly used methods for pile testing due to its relatively low cost and minimal pile preparation requirements.

The testing is carried out after the foundation has been installed and cured. Elastic waves are generated by striking the top of the pile with a handheld hammer. These waves travel down the pile shaft and are reflected back from the pile toe or any irregularities, such as changes in cross-section, variations in elastic modulus, or differences in material density. The reflected waves are detected by an accelerometer or velocimeter positioned at the top of the pile. The collected signals, representing acceleration or velocity over time, are then processed and prepared for interpretation.

To determine the pile's length and integrity, one must analyze the features in the processed signals (e.g., relative velocity changes after the initial impact pulse), along with site records, soil profiles, and other relevant data. The pile length or distance to the defect L is calculated using the Equation:

$$L = \frac{V \cdot \Delta t}{2} \quad (1)$$

where V represents the wave speed, assumed to be a constant value (usually 3600 - 4400 m/s for concrete piles) and Δt is the time taken for the waves to travel from the pile head to the reflector and back. A clear reflection from the pile toe and a sufficiently stable signal generally indicates a defect-free pile.

However, low strain integrity testing is constrained by several limitations, as highlighted in Amir [11] and Chai & Phoon [42]:

- The method often fails to detect minor inclusions or cross-sectional changes of less than 25%.
- The accuracy of the test is significantly affected by the pile's length-to-diameter ratio and the surrounding soil's elastic properties. Accurate length determination is usually possible within length-to-diameter ratios ranging from 20 (in hard soils) to 60 (in very soft soils).
- The pile length and the distance to detected anomalies are linearly dependent on the assumed wave speed, which can introduce errors of about 10%.
- The test typically does not provide information on the pile's integrity beyond the first significant signal anomaly.
- The test offers limited insight into the upper portion of the pile and cannot detect defects near the pile toe within approximately 10% of the pile's length.

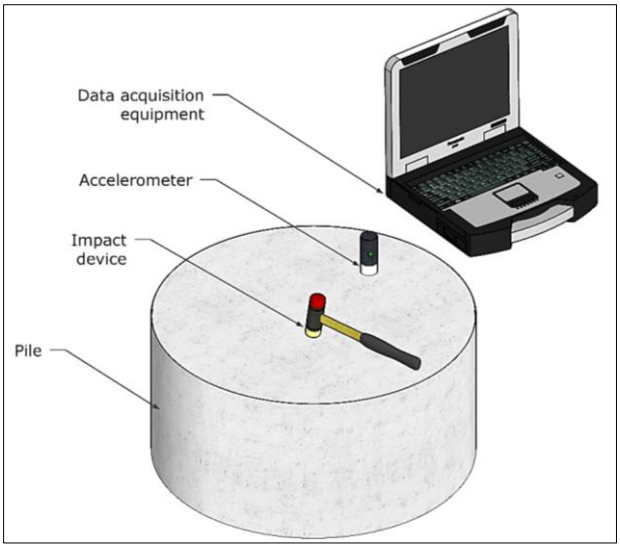

Figure 2. Low strain impact integrity test arrangement

2.3. Field Low Strain Integrity Testing of Piles with Artificial Defects

As mentioned in the previous section, the professional consensus is that defects occupying less than 25% of the pile cross-section may go undetected by low strain integrity tests. To investigate this limitation, gather the necessary data, and explore methods to identify the weak responses from small defects, we conducted a study involving real-life testing of piles with artificially induced defects, followed by subsequent numerical simulations.

For the real-life testing, we constructed ten cast-in-place piles, each with a diameter of 450 mm and a length of 3 m (Figure 3). The experimental setup included one defect-free pile (No. 1) and nine piles with artificial defects of various dimensions: three with a Ø250×100 mm defect (Nos. 2, 3, 4), three with a 100×150×300 mm defect (Nos. 5, 6, 7), and three with a 100×150×150 mm defect (Nos. 8, 9, 10). These defects were made of polystyrene (Figure 4), chosen for its significantly lower elastic properties compared to concrete, which allows for effective wave reflection and robust binding to the reinforcement cages. The defects were designed to replicate common pile issues such as soil inclusions or washouts.

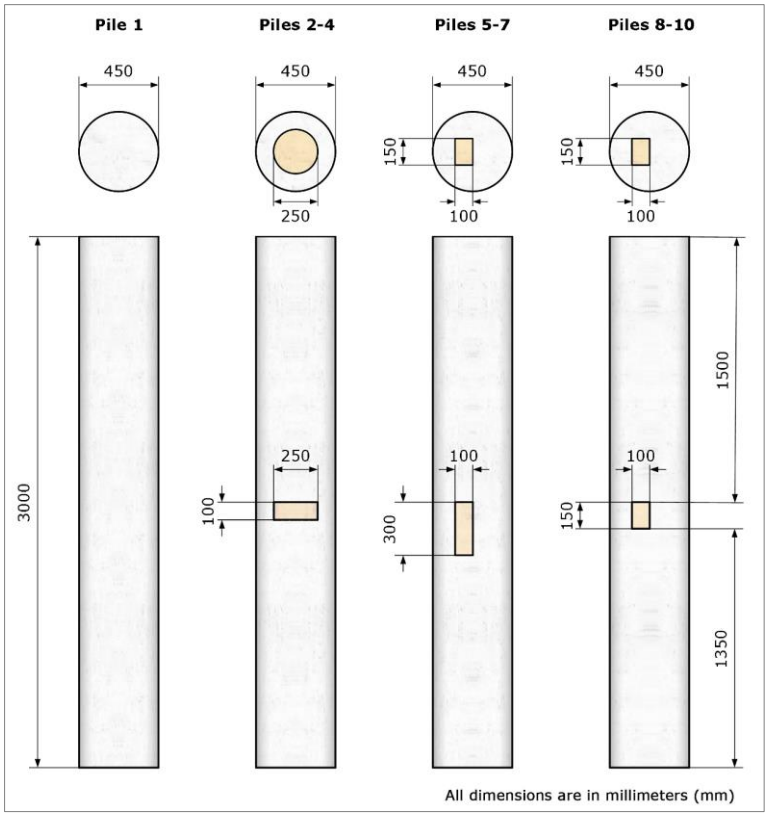

Figure 3. Layouts of piles with artificial defects

Figure 4. Artificial defects with dimensions: Ø250×100 mm, 100×150×150 mm, and 100×150×300 mm (from left to right)

The reinforcement cages were constructed to be 3 meters long, using six longitudinal reinforcement bars with a diameter of Ø18 mm. The inner diameter of each cage was 250 mm. The artificial defects were securely fastened to the reinforcement cages using binding wire, precisely centered within the cage (Figure 5).

Figure 5. Reinforcement cages before (1st row) and after (2nd row) the installation of defects

The construction of the piles was carried out using Continuous Flight Auger (CFA) technology, which involved drilling, concreting, and reinforcing the shafts with the cages containing the artificial defects (Figure 6). A detailed log of the drilling, concreting, and reinforcement processes was meticulously maintained throughout the construction of the experimental site.

Low strain integrity testing on piles with artificial defects was performed seven days after casting. Before testing, the pile head surfaces were cleaned, and sound concrete areas were prepared to facilitate the excitation of elastic waves and accurate data acquisition. An accelerometer from the Interpribor Spektr-4 equipment set was attached sequentially at three different locations on the pile top, using a small amount of putty to ensure proper coupling between the sensor and the pile head. At each location, a series of at least five light impacts was applied using a hammer with a soft plastic head, weighing approximately 0.5 kg (Figure 6). The resulting acceleration data were processed by integrating over time, shifting, amplifying, normalizing to the maximum value, and plotting using custom-developed Python software.

Figure 6. Construction of piles with defects

The results for each pile, including one flawless pile and three with each type of defect, along with their respective layouts, are given in Figure 7. All processed signals showed a distinct reflection from the pile toe, observed at a timestamp of 1.5–1.7 ms, which is consistent with a 3-meter pile length and an assumed wave speed of 3550–4000 m/s. However, the time-domain analysis of the signals revealed no detectable variations corresponding to the artificially induced defects in the test piles. Consequently, while the testing successfully confirmed the pile lengths, it failed to identify any defects. Following the measurements, the test piles were immediately buried, precluding any further field studies.

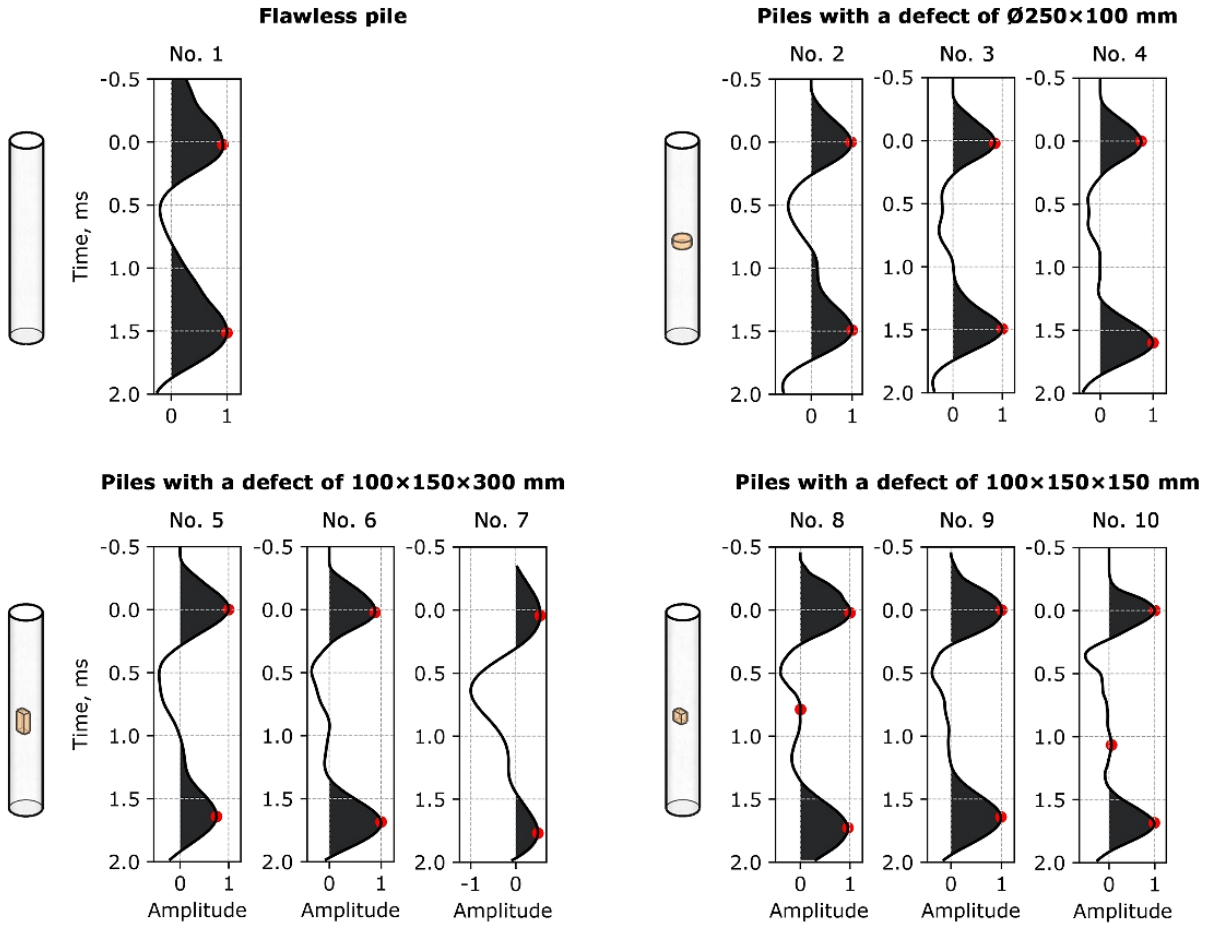

Figure 7. Results of field low strain integrity testing and layouts of the tested piles with artificial defects. Hereafter, red dots indicate the local maxima of the signals

2.4. Numerical Simulations

To validate the field test results, a series of three-dimensional numerical simulations were performed using COMSOL Multiphysics 5.3 and the finite element method [38]. We modeled four scenarios to replicate the piles with artificial defects described earlier (Figure 3): Model 1 for a flawless pile, Model 2 for a pile with a Ø250×100 mm defect, Model 3 for a pile with a 100 × 150 × 300 mm defect, and Model 4 for a pile with a 100 × 150 × 150 mm defect.

The simulations aimed to examine how elastic wave fields evolve over space and time based on the predefined model parameters. The properties of the simulated materials [38, 43] were characterized by density (ρ), pressure wave speed (V_P), shear wave speed (V_S), and Rayleigh damping coefficients α and β [44-46], as given in Table 1. The surrounding medium for the piles was modeled as sand [47, 48].

Table 1. Material properties

Properties	Concrete	Surrounding soil (sand)	Polystyrene
Density ρ, kg/m^3	2400	1500	1060
Longitudinal wave speed V_P, m/s	4000	600	2350
Shear wave speed V_S, m/s	2450	200	1120
Rayleigh coefficients: α, s^{-1}; β, s	20; 10^{-8}	200; 10^{-7}	2000; 10^{-6}

Figure 8 presents the results of numerical simulations for all models and input force pulse durations (0.5, 0.75, 1, and 1.2 ms). Each synthetic velocity trace reveals a distinct reflection from the pile toe. Sensitivity to defects varies with pulse duration: longer pulses are less sensitive to defects, while shorter pulses provide clearer reflections, particularly in Model 2. For Models 3 and 4, very minor signal features appear at the expected times for defect reflections but are difficult to interpret definitively.

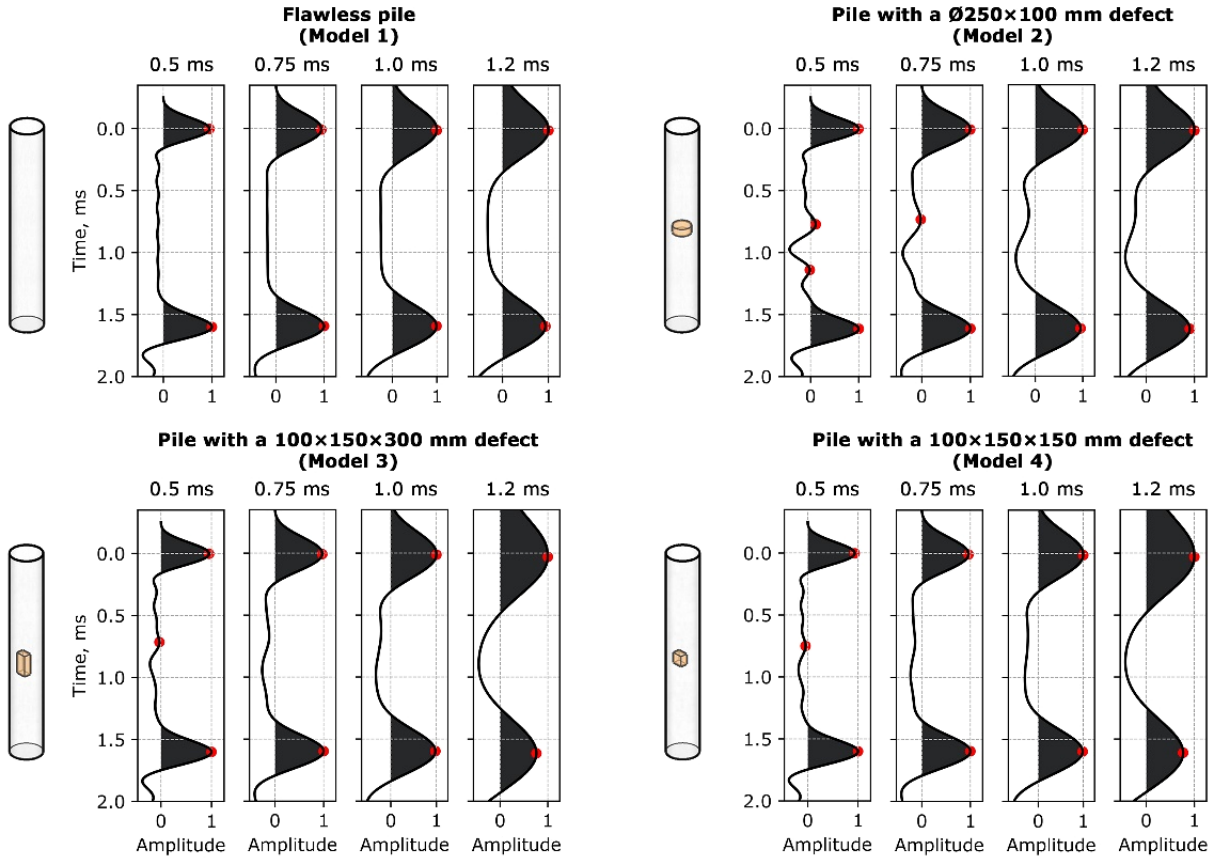

Figure 8. Results of low strain integrity test simulations with input force pulses of 0.5, 0.75, 1, and 1.2 ms along with layouts of the models

The results from simulations with long-duration pulses are consistent with experimental findings (Figure 7). However, even with shorter pulses, the synthetic tests did not successfully identify defects in Models 3 and 4. To improve the detection of subtle defect responses, which are nearly invisible in the time domain, we will extend the study by applying CCWT for time-frequency analysis.

Elastic waves were generated by applying an initial vertical force *F*, modeled as a Gaussian pulse modulated by a Hanning window, to a 45 mm diameter impact area at the center of the pile top. This force is described by the Equation:

$$F(t) = -A\mathrm{e}^{-2\pi\left(\frac{t-0.5T}{T}\right)^2} \cdot \begin{Bmatrix} 0.5\left(1-\cos\left(2\pi\frac{t}{T}\right)\right) & if\ 0 < t < T \\ 0 & \text{otherwise} \end{Bmatrix} \quad (2)$$

where *A* is the maximum force value, *t* is the time, and *T* is the characteristic pulse duration. The velocity response of each pile was recorded across its entire top using a synthetic sensor (velocimeter) to capture and average data from all possible sensor positions. To improve the resolution of the low strain test, different hammers with varying weights and head materials can be used, as detailed in the Loseva et al. [38]. To replicate the effects of the different hammers in our simulations, we conducted four separate calculations for each model, using input force pulse durations of 0.5, 0.75, 1, and 1.2 ms.

The finite element mesh was composed of both mapped and triangular (tetrahedral in 3D) elements [49-51]. The maximum size of a finite element did not exceed 10% of the minimum wavelength of the simulated elastic wave, generally around 1 cm. In areas requiring higher accuracy, the element size was reduced to 1 mm. The simulation time was set to 10 ms, with time discretization based on the spatial mesh size. A time step of 0.5 μs was used, in line with the Courant-Friedrichs-Lewy criterion. To avoid reflections from the external boundaries of the model, low-reflecting boundary conditions were applied to the side and bottom boundaries of the surrounding soil.

2.5. Application of CCWT for Low Strain Integrity Testing

To distinguish weak reflections from minor defects, we will analyze the time-frequency spectrum of the acquired signals using the CCWT technique [31–33, 35]. The CCWT converts the input signal $f(t) \in L^2(R)$ into a function of two variables $a, b \in R$, $a > 0$:

$$W(a,b) = \int_{-\infty}^{+\infty} f(t)\frac{1}{\sqrt{a}}\psi^*\left(\frac{t-b}{a}\right)dt \quad (3)$$

where $\psi(t)$ is the complex mother wavelet, * denotes the complex conjugate, a is the scale parameter of the mother wavelet, and b represents the time shift that positions the wavelet.

The scale parameter a can be converted to frequency (or pseudo-frequency) f using the following Equation:

$$\mathrm{f} = \frac{\mathrm{f_c}}{\mathrm{a}\cdot\Delta\mathrm{t_S}} \quad (4)$$

where f_c is the center frequency of the mother wavelet (dimensionless) and Δt_S is the sampling period.

For our analysis, we use the complex Morlet wavelet as the mother wavelet, which consists of a complex sinusoid modulated by a Gaussian envelope:

$$\psi(\mathrm{t}) = \frac{1}{\sqrt{\pi \mathrm{B}}}\mathrm{e}^{-\frac{\mathrm{t}^2}{\mathrm{B}}}\mathrm{e}^{\mathrm{i}2\pi\mathrm{Ct}} \quad (5)$$

where *B* is the bandwidth and *C* is the center frequency. The complex Morlet wavelet facilitates a clear decomposition of the test data, highlighting specific features of interest as individual anomalies [48]. By adjusting parameters *B* and *C*, we can tailor the mother wavelet to signals from input force pulses of various durations and refine the time-frequency resolution of the wavelet transform.

As the wavelet function is complex-valued, the corresponding wavelet transform $W(a,b)$ can be divided into its real part $\mathrm{W_R}(a,b)$ and imaginary part $\mathrm{W_I(a,b)}$, or into its amplitude $|W(a,b)|$ and phase (or phase-angle) $\varphi(\mathrm{a,b})$, which is calculated as:

$$\varphi(\mathrm{a,b}) = \arctan\left(\frac{\mathrm{W_I(a,b)}}{\mathrm{W_R(a,b)}}\right) \quad (6)$$

The phase angles of the wavelet coefficients can be visualized as a time-frequency domain image (phase spectrum), where phase angle values are depicted using a color scale. This image features a linear horizontal axis for time (the time shift, b) and a logarithmic vertical axis for frequency f.

To locate the pile toe or defects, Ni et al. [28-31] suggested identifying phase shifts from 180° (π) to -180° (-π), which appear as a straight line transitioning from higher to lower frequencies in the phase spectrum. The initial phase shift represents the input force pulse, while subsequent shifts correspond to reflections from the pile toe or defects. The

time difference between these lines can be converted to depth using Equation 1. The CCWT phase spectrum analysis provides a significant advantage by revealing even small, low-amplitude signal features with distinct frequency responses that may not be apparent through traditional time-domain analysis or wavelet transform amplitude analysis.

3. Results

3.1. CCWT Analysis of the Numerical Simulation Results

We proceed with the CCWT analysis of the synthetic signals obtained from numerical simulations (refer to Section 2.4). For this analysis, we employed the complex Morlet wavelet as the mother wavelet, with bandwidth and center frequency parameters set at 0.12 and 1.5, respectively. These settings were uniformly applied across all input force pulse durations to ensure comparability.

In practical scenarios, bandwidth and center frequency parameters may need to be fine-tuned for each analyzed signal and impact hammer used. The analyst can adjust the parameters interactively based on several criteria: features that are clearly identifiable in the time-domain should be accurately represented in the time-frequency domain in both amplitude and phase wavelet spectra; the wavelet spectra should be free of artifacts at the start and end of the signal; and the characteristics of the phase spectrum should be consistent across signals from different hammer blows and receiver positions, ensuring that observed features are not influenced by noise.

Figure 9 shows the synthetic velocity traces for all models and input pulse durations, along with their corresponding CCWT phase spectra. Distinct time-domain features in the velocity traces, observed at 0 ms and 1.6 ms—corresponding to the hammer impact and the response from the pile toe, respectively—are clearly identified in the phase spectra. These features appear as well-localized straight lines in both the time and frequency domains, with phase shifts transitioning from π to -π and spanning frequencies from approximately 500 Hz to 10,000 Hz.

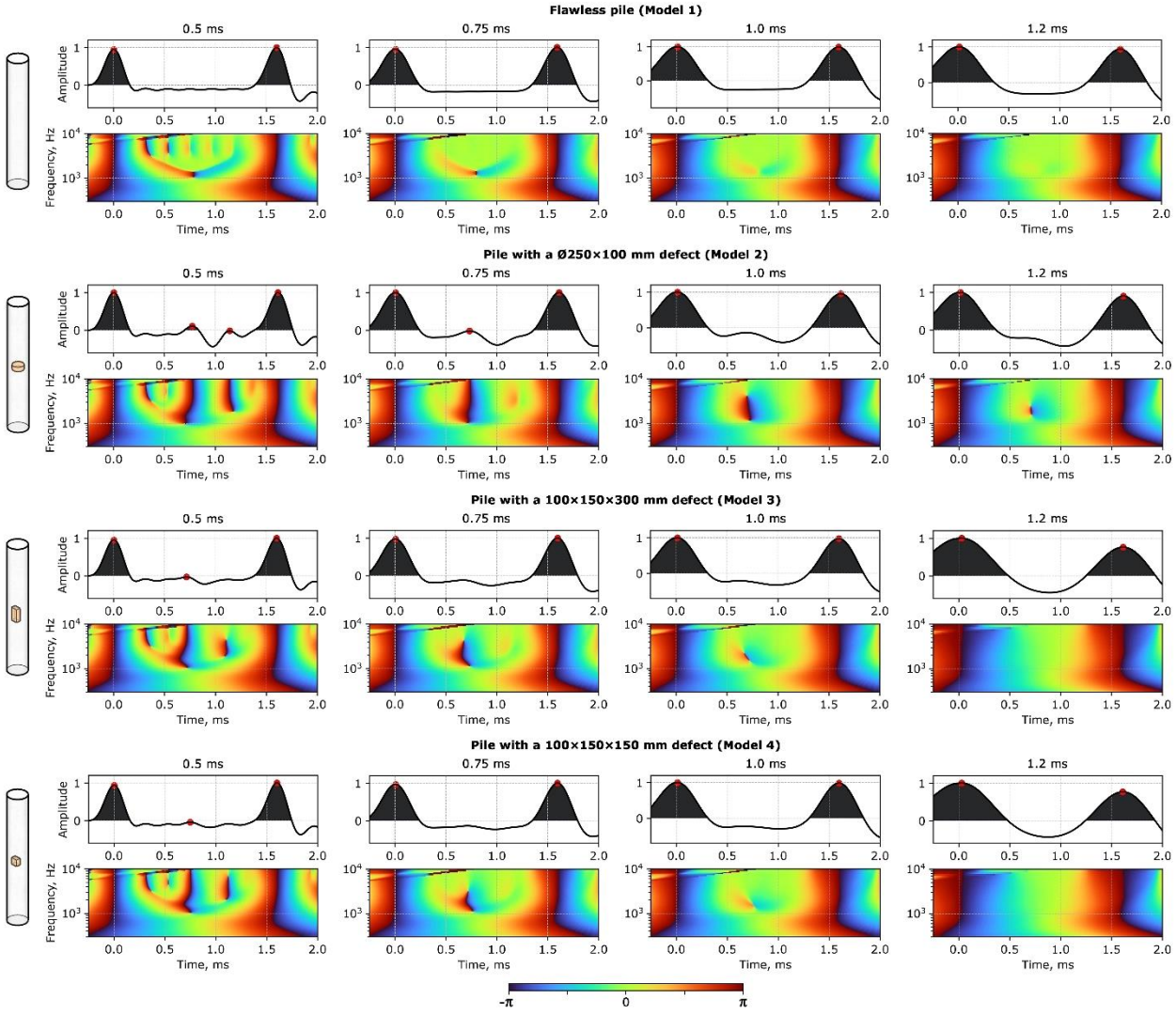

Figure 9. CCWT of low strain integrity test simulation results: synthetic velocity traces and corresponding CCWT phase spectra. The color scale indicates phase angle values

For piles with defects (Models 2-4), notable phase shifts from π to -π, spanning high to low frequencies around 0.75 ms, are also observed. These features are consistent across different input force durations for each model, although some variations (not evident for the longest 1.2 ms pulse in Models 3 and 4) can be attributed to the sensitivity differences of low- and high-frequency signal excitations. These phase shifts, occurring at the expected timestamps, are interpreted as responses from small defects predefined in the numerical models. While these defects may not be clearly distinguishable in the time domain, they are distinctly observable through the more sensitive CCWT phase spectrum analysis.

3.2. CCWT Analysis of Field Low Strain Integrity Testing Data

The CCWT analysis techniques, previously applied to synthetic signals, were utilized for the field low strain integrity test data from piles with artificial defects (see Section 2.3). As expected, the CCWT phase spectra for each of the 10 tested piles clearly reveal the time-domain pulses corresponding to hammer impacts and responses from the pile toe. These are marked by phase shifts from π to -π across frequencies ranging from approximately 800 to 10,000 Hz (Figure 10).

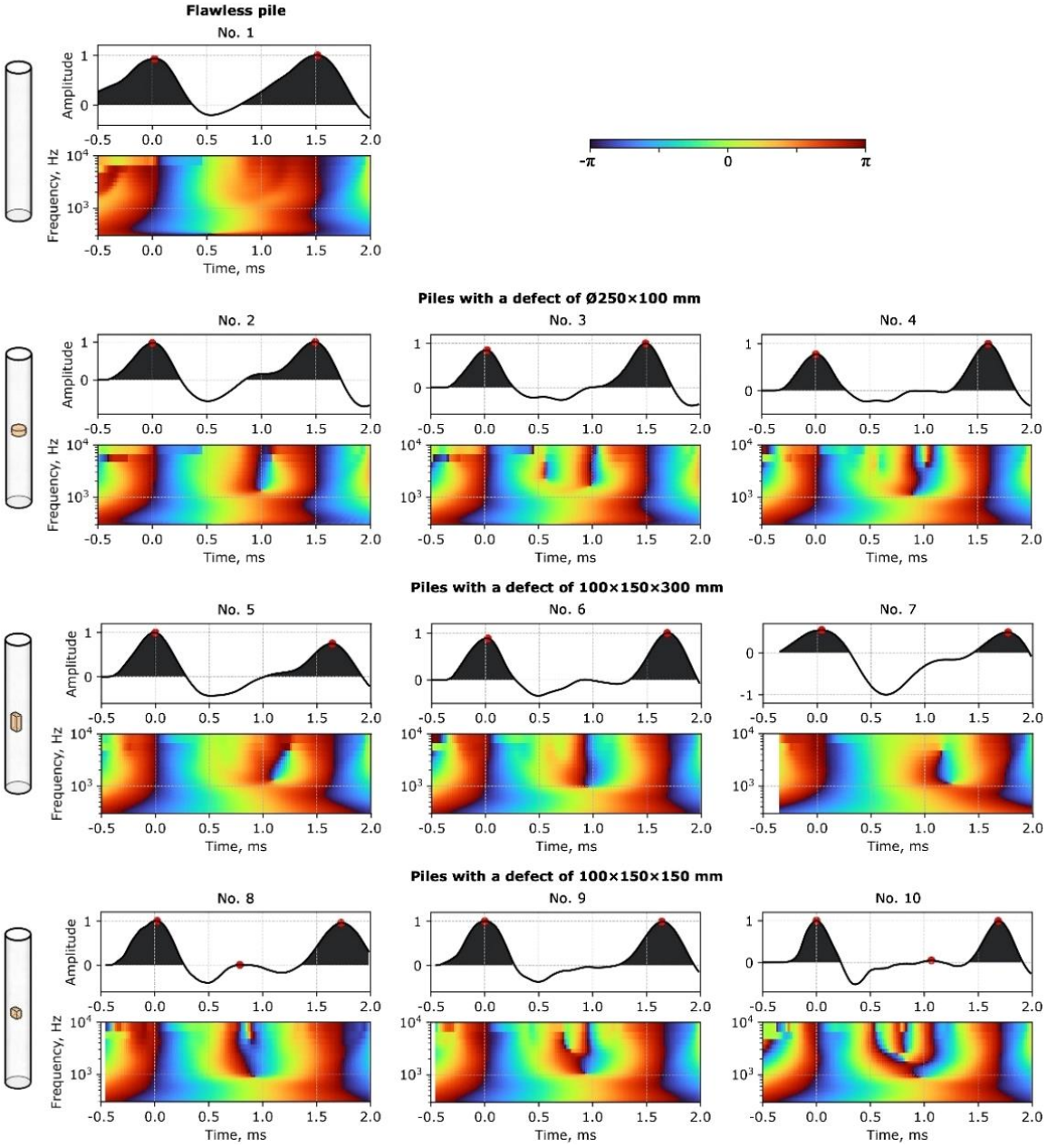

Figure 10. CCWT of field low strain integrity testing results: velocity traces and corresponding CCWT phase spectra. The color scale indicates phase angle values

For a flawless pile, the phase spectra display only these two characteristic shifts. In contrast, piles with pre-installed defects exhibit additional features around the 0.8–1.0 ms timestamps. These features manifest as phase shifts transitioning from high to low frequencies, indicating the presence of small artificial defects installed within the piles.

The CCWT analysis of the field data aligns with the results from numerical simulations, confirming the validity of both the proposed methodology and the simulation procedures. However, it is important to note that in the field data, pulses from the pile toe and defects arrived slightly later than expected, with some variation in arrival times between piles. This delay is likely attributed to installation imperfections, such as overdrilling, and the three-dimensional effects of wave propagation – specifically, the reduced speed of wave propagation in semispherical patterns near the pile head [52]. Such variations are more pronounced in the shorter piles tested and are anticipated to be less significant in longer piles, which are more typical in real-world applications.

Fine-tuning the bandwidth and center frequency parameters of the complex Morlet wavelet for each collected signal can slightly improve defect localization and provide clearer phase spectrum features. However, for consistency, we used the same parameters for all signals in our study to avoid overfitting and ensure reliable results. Therefore, the fine-tuning results are not presented here.

4. Conclusions

Minor flaws in piles can significantly compromise their structural capacity, underscoring the importance of early and accurate detection. Traditional methods for analyzing low strain impact testing results are generally effective at identifying major defects, leaving smaller yet potentially critical flaws undetected. This limitation underscores the need for more sensitive techniques capable of detecting and localizing minor defects, thereby ensuring the long-term safety of pile foundations. Our study addresses this issue by proposing a refined low strain impact testing workflow, based on real-life tests of piles with artificially introduced defects and validated through numerical simulations.

The refined workflow, detailed in the flowchart (Figure 11), employs a set of hammers with different weights and head materials for data collection, followed by a time-frequency analysis of the CCWT phase spectra of the collected signals. Different hammer configurations provide varied wave excitation frequencies, resulting in diverse sensitivities to inhomogeneities within the piles and distinct noise patterns. The subsequent CCWT phase analysis reveals minor signal changes associated with small flaws through characteristic phase shifts ranging from high to low frequencies. The consistency of these phase features across signals collected with different hammers (considering their varying sensitivities) aids in distinguishing genuine flaw-induced phase shifts from noise or other unrelated factors. Despite the promising results, further research is needed to test the approach on piles with larger length-to-diameter ratios and those installed in harder soils, as these conditions may produce more complex phase spectra that are more difficult to interpret. The use of different hammers is expected to help address these complexities.

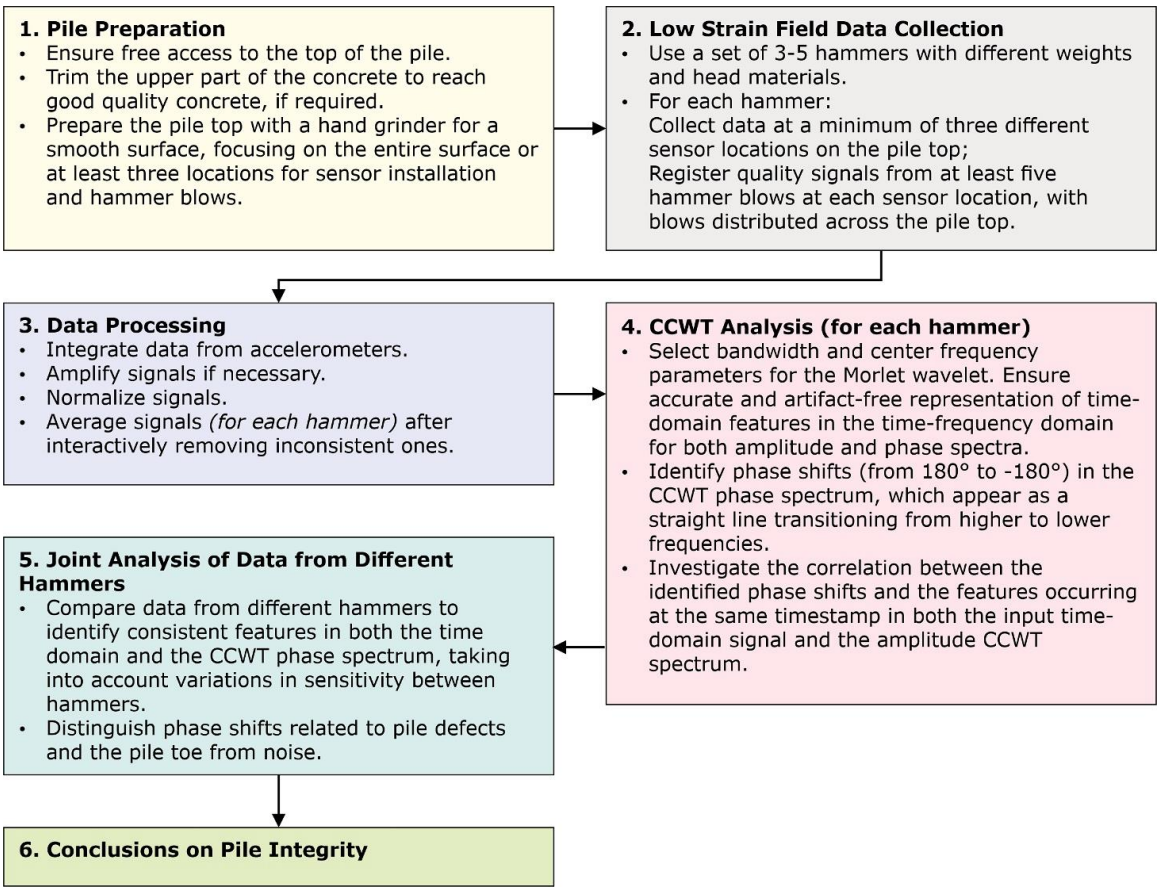

Figure 11. Low strain pile integrity testing workflow, refined for enhanced accuracy in detecting minor flaws

5. Declarations

5.1. Author Contributions

Conceptualization, E.L. and I.L.; methodology, I.L.; software, I.L. and R.Z.; validation, I.L., R.Z., and E.L.; formal analysis, I.L., R.Z., and E.L.; investigation, I.L., E.L., and R.Z.; resources, E.L. and R.Z.; data curation, I.L., R.Z., and E.L.; writing—original draft preparation, E.L.; writing—review and editing, I.L. and R.Z.; visualization, I.L.; supervision, I.L.; project administration, E.L. and I.L. All authors have read and agreed to the published version of the manuscript.

5.2. Data Availability Statement

The data presented in this study are available on request from the corresponding author.

5.3. Funding

The authors received no financial support for the research, authorship, and/or publication of this article.

5.4. Conflicts of Interest

The authors declare no conflict of interest.

6. References

[1] Fleming, K., Weltman, A., Randolph, M., & Elson, K. (2008). Piling Engineering. CRC Press, Boca Raton, United States. doi:10.1201/b22272.

[2] Shammazov, I. A., Batyrov, A. M., Sidorkin, D. I., & Van Nguyen, T. (2023). Study of the Effect of Cutting Frozen Soils on the Supports of Above-Ground Trunk Pipelines. Applied Sciences (Switzerland), 13(5), 3139. doi:10.3390/app13053139.

[3] Lavrik, A., Buslaev, G., & Dvoinikov, M. (2023). Thermal Stabilization of Permafrost Using Thermal Coils inside Foundation Piles. Civil Engineering Journal (Iran), 9(4), 927–938. doi:10.28991/CEJ-2023-09-04-013.

[4] Syas'ko, V., & Shikhov, A. (2022). Assessing the State of Structural Foundations in Permafrost Regions by Means of Acoustic Testing. Applied Sciences (Switzerland), 12(5), 2364. doi:10.3390/app12052364.

[5] Blinov, P. A., Shansherov, A. V., Cheremshantsev, D. M., Kuznetsova, N. Y., & Nikishin, V. V. (2022). Analysis and Selection of a Grouting Mixture, Resistant to Dynamic Loads, in Order to Improve the Support Tightness Quality in the Annulus. Bulletin of the Tomsk Polytechnic University, Geo Assets Engineering, 333(11), 115–123. doi:10.18799/24131830/2022/11/3726.

[6] Dvoynikov, M. V., Nikitin, V. I., & Kopteva, A. I. (2024). Analysis of Methodology for Selecting Rheological Model of Cement Slurry for Determining Technological Parameters of Well Casing. International Journal of Engineering, Transactions B: Applications, 37(10), 2042–2050. doi:10.5829/ije.2024.37.10a.15.

[7] Petrakov, D. G., Loseva, A. V., Jafarpour, H., & Penkov, G. M. (2024). Experimental Evaluation of Effective Chemical Composition on Reservoir Quality of Bottomhole Zone of Low Permeability Terrigenous Reservoirs. International Journal of Engineering, Transactions B: Applications, 37(8), 1547–1555. doi:10.5829/IJE.2024.37.08B.08.

[8] Kuzmin, A. M., Buslaev, G. V., Morenov, V. A., Tseneva, S. N., & Gavrilov, N. (2022). Improving the energy-efficiency of small-scale methanol production through the use of microturboexpander units. Journal of Mining Institute, 258, 1038–1049. doi:10.31897/PMI.2022.104.

[9] Amir, J. M. (2017). Pile integrity testing: history, present situation and future agenda. The 3rd International Conference on Deep Foundations, 27-29 April, Santa Cruz de la Sierra, Bolivia.

[10] Gao, T. (2022). A Critical Analysis of Existing Intelligent Analytical Techniques for Pile Integrity Test. 2022 8th International Conference on Hydraulic and Civil Engineering: Deep Space Intelligent Development and Utilization Forum (ICHCE), 740–751. doi:10.1109/ichce57331.2022.10042772.

[11] Amir, J. M. (2020). Pile integrity testing: all about the methods of pile NDT (2nd Ed.). Piletest.com, Hemel Hempstead, United Kingdom.

[12] ASTM D582-16. (2016). Standard Test Method for Low Strain Impact Integrity Testing of Deep Foundations. ASTM International, Pennsylvania, United States. doi:10.1520/d5882-16.

[13] Sarhan, H. A., O'Neill, M. W., & Tabsh, S. W. (2004). Structural capacity reduction for drilled shafts with minor flaws. Structural Journal, 101(3), 291-297. doi:10.14359/13088.

[14] Iskander, M., Roy, D., Kelley, S., & Ealy, C. (2003). Drilled Shaft Defects: Detection, and Effects on Capacity in Varved Clay. Journal of Geotechnical and Geoenvironmental Engineering, 129(12), 1128–1137. doi:10.1061/(asce)1090-0241(2003)129:12(1128).

[15] Debnath, L., & Bhatta, D. (2014). Integral Transforms and Their Applications. Chapman and Hall/CRC, New York, United States. doi:10.1201/b17670.

[16] Debnath, L., & Shah, F. A. (2015). Brief Historical Introduction. Wavelet Transforms and Their Applications. Birkhäuser, Boston, United States. doi:10.1007/978-0-8176-8418-1_1.

[17] Sejdić, E., Djurović, I., & Jiang, J. (2009). Time–frequency feature representation using energy concentration: An overview of recent advances. Digital Signal Processing, 19(1), 153–183. doi:10.1016/j.dsp.2007.12.004.

[18] Grossmann, A., & Morlet, J. (2009). Decomposmon of hardy functions into square integrable wavelets of constant shape. Fundamental Papers in Wavelet Theory, 15(4), 126–139. doi:10.1515/9781400827268.126.

[19] Ali, A., Sheng-Chang, C., & Shah, M. (2020). Continuous wavelet transformation of seismic data for feature extraction. SN Applied Sciences, 2(11), 1-12. doi:10.1007/s42452-020-03618-w.

[20] Palupi, I. R. (2018, April). Depth prediction of gravity data by using continous wavelet transform. EAGE-HAGI 1st Asia Pacific Meeting on Near Surface Geoscience and Engineering, European Association of Geoscientists & Engineers, 1-4.

[21] Deleersnyder, W., Hermans, T., & Dudal, D. (2024). An efficient workflow for airborne electromagnetic data processing for advanced applications. Copernicus Meetings: No. EGU24-16111. doi:10.5194/egusphere-egu24-16111.

[22] Chatterjee, P. (2018). Wavelet Analysis in Civil Engineering. CRC Press, London, United Kingdom. doi:10.1201/b18057.

[23] Saadatmorad, M., Khatir, S., Cuong-Le, T., Benaissa, B., & Mahmoudi, S. (2024). Detecting damages in metallic beam structures using a novel wavelet selection criterion. Journal of Sound and Vibration, 578, 118297. doi:10.1016/j.jsv.2024.118297.

[24] Thoriya, A., Vora, T., Jadeja, R., Ali Abdelrahman Ali, Y., & Patel, S. K. (2024). Application of wavelet transform techniques for corrosion assessment of embedded rebars in RC elements using electromechanical impedance. Measurement: Journal of the International Measurement Confederation, 226, 114081. doi:10.1016/j.measurement.2023.114081.

[25] Addison, P. S., & Watson, J. N. (1997). Wavelet analysis for low strain integrity testing of foundation piles. 5th International conference on inspection, appraisal, repairs, maintenance of buildings and structures, 15-16 May, 1997, Singapore.

[26] Watson, J. N., Addison, P. S., & Sibbald, A. (1999). De-noising of sonic echo test data through wavelet transform reconstruction. Shock and Vibration, 6(5), 267–272. doi:10.1155/1999/175750.

[27] Wang, J. (2003). Wavelet analyses for stress wave detection of piles. Science in China Series E, 46(2), 113. doi:10.1360/03ye9011.

[28] Ni, S. H., Isenhower, W. M., & Huang, Y. H. (2012). Continuous wavelet transform technique for low-strain integrity testing of deep drilled shafts. Journal of GeoEngineering, 7(3), 97–105. doi:10.6310/jog.2012.7(3).3.

[29] Ni, S. H., Yang, Y. Z., Tsai, P. H., & Chou, W. H. (2017). Evaluation of pile defects using complex continuous wavelet transform analysis. NDT and E International, 87, 50–59. doi:10.1016/j.ndteint.2017.01.007.

[30] Ni, S. H., Yanga, Y. Z., & Lyu, C. R. (2017). Application of wavelet transform for the impulse response of pile. Smart Structures and Systems, 19(5), 513–521. doi:10.12989/sss.2017.19.5.513.

[31] Ni, S. H., Li, J. L., Yang, Y. Z., & Lai, Y. Y. (2019). Applicability of complex wavelet transform to evaluate the integrity of commonly used pile types. Journal of GeoEngineering, 14(1), 21–30. doi:10.6310/jog.201903_14(1).3.

[32] Zheng, W., Zheng, W., Wang, S., Lin, C., Yu, X., & Liu, J. (2020). Damage Localization of Piles Based on Complex Continuous Wavelet Transform: Numerical Example and Experimental Verification. Shock and Vibration, 2020, 1–9. doi:10.1155/2020/8058640.

[33] Liu, J. L., Lin, C. X., Ye, X. J., Zheng, W. T., & Luo, Y. P. (2021). An improved algorithm for pile damage localization based on complex continuous wavelet transform. Smart Structures and Systems, 27(3), 493–506. doi:10.12989/sss.2021.27.3.493.

[34] Churkin, A. A., Ulybin, A. V., & Kapustin, V. V. (2021). Application of low strain impact testing to spliced driven piles quality control. Stroitel'stvo Unikal'nyh Zdanij i Sooruzenij, (3), 1-14.

[35] Loseva, E., Lozovsky, I., Zhostkov, R., & Syasko, V. (2022). Wavelet Analysis for Evaluating the Length of Precast Spliced Piles Using Low Strain Integrity Testing. Applied Sciences (Switzerland), 12(21), 10901. doi:10.3390/app122110901.

[36] Ponomaryov, A. B., Zakharov, A. V., Tatyannikov, D. A., & Shalamova, E. A. (2023). Geotechnical Monitoring in the Urban Construction Environment. Soil Mechanics and Foundation Engineering, 60(5), 452–458. doi:10.1007/s11204-023-09914-y.

[37] Zakharov, A. V., Ponomaryov, A. B., & Ofrikhter, I. V. (2022). Model of soil thermal conductivity in the form of a truncated sphere. Magazine of Civil Engineering, 114(6), 11403. doi:10.34910/MCE.114.3.

[38] Loseva, E., Lozovsky, I., & Zhostkov, R. (2022). Identifying Small Defects in Cast-in-Place Piles Using Low Strain Integrity Testing. Indian Geotechnical Journal, 52(2), 270–279. doi:10.1007/s40098-021-00583-y.

[39] Vinogradova, A., Gogolinskii, K., Umanskii, A., Alekhnovich, V., Tarasova, A., & Melnikova, A. (2022). Method of the Mechanical Properties Evaluation of Polyethylene Gas Pipelines with Portable Hardness Testers. Inventions, 7(4), 125. doi:10.3390/inventions7040125.

[40] Schipachev, A. M., & Aljadly, M. (2023). Magnetic-Pulsed Treatment to Improve the Strength Properties of Defective Sections of Oil and Gas Pipelines. Bulletin of the Tomsk Polytechnic University, Geo Assets Engineering, 334(5), 7–16. doi:10.18799/24131830/2023/5/4011.

[41] Alekhnovich, V., Syasko, V., & Umanskii, A. (2024). Multi-Parameter Complex Control of Metal Coatings on Ball Plugs of Pipeline Shut-Off Valves. Inventions, 9(4), 78. doi:10.3390/inventions9040078.

[42] Chai, H.-Y., & Phoon, K.-K. (2013). Detection of Shallow Anomalies in Pile Integrity Testing. International Journal of Geomechanics, 13(5), 672–677. doi:10.1061/(asce)gm.1943-5622.0000233.

[43] Zhostkov, R.A. (2019). A Software for Simulation of Low Integrity Testing for Cast-in-Place Piles. Patent RF. 2019.665449.

[44] Lozovsky, I. N., Zhostkov, R. A., & Churkin, A. A. (2020). Numerical Simulation of Ultrasonic Pile Integrity Testing. Russian Journal of Nondestructive Testing, 56(1), 1–11. doi:10.1134/S1061830920010064.

[45] Warburton, G. B. (1995). Dynamics of structures, by Ray W. Clough and Joseph Penzien, 2nd edition, McGraw-Hill, New York, United Sttaes. Earthquake Engineering & Structural Dynamics, 24(3), 457–462. doi:10.1002/eqe.4290240311.

[46] Stojić, D., Nestorović, T., Marković, N., & Marjanović, M. (2018). Experimental and numerical research on damage localization in plate-like concrete structures using hybrid approach. Structural Control and Health Monitoring, 25(9), 2214. doi:10.1002/stc.2214.

[47] Lide, D. R. (2004). CRC handbook of chemistry and physics. CRC Press, London, United Kingdom.

[48] Briaud, J. L. (2023). Geotechnical engineering: unsaturated and saturated soils. John Wiley & Sons, Hoboken, United States.

[49] Vasilyeva, N. V., Boikov, A. V., Erokhina, O. O., & Trifonov, A. Y. (2021). Automated digitization of radial charts. Journal of Mining Institute, 247(1), 82–87. doi:10.31897/PMI.2021.1.9.

[50] Belyakov, N., Smirnova, O., Alekseev, A., & Tan, H. (2021). Numerical simulation of the mechanical behavior of fiber-reinforced cement composites subjected dynamic loading. Applied Sciences (Switzerland), 11(3), 1–15. doi:10.3390/app11031112.

[51] Basalaeva, P. B., & Kuranov, A. D. (2024). Influence of dip angle of lithologically non-uniform interburden on horizontal mine opening stability during driving. Mining Informational and Analytical Bulletin, (3), 17–30. doi:10.25018/0236_1493_2024_3_0_17.

[52] Liu, X., Hesham EI Naggar, M., Wang, K., & Wu, W. (2020). Theoretical analysis of three-dimensional effect in pile integrity test. Computers and Geotechnics, 127, 103765. doi:10.1016/j.compgeo.2020.103765.